ISSN 0015-4628, Fluid Dynamics, 2016, Vol. 51, No. 3, pp. 299–310. © Pleiades Publishing, Ltd., 2016.
Original Russian Text © M.E. Eglit, A.E. Yakubenko, 2016, published in Izvestiya Rossiiskoi Akademii Nauk, Mekhanika Zhidkosti i Gaza, 2016, Vol. 51, No. 3, pp. 3–15.

Effect of the Bottom Material Capture and the Non-Newtonian Rheology on the Dynamics of Turbulent Downslope Flows

M. E. Eglit[a] and A. E. Yakubenko[b]

[a]*Lomonosov Moscow State University, Faculty of Mechanics and Mathematics, Leninskiye Gory 1, Moscow, 119991 Russia*

[b]*Institute of Mechanics, Lomonosov Moscow State University, Michurinskii pr. 1, Moscow, 119192 Russia*

e-mail: m.eglit@mail.ru, yakub@imec.msu.ru

Received September 14, 2015

Abstract—The paper is devoted to the mathematical modeling of naturally occurring downslope flows, such as snow avalanches, mudflows, and rapid landslides. The medium in motion is modeled as a non-Newtonian fluid, the non-Newtonian fluids of different types corresponding to different-in-nature flows. It is taken into account that the downslope flows capture the slope material and entrain it into the motion. The flow is assumed to be turbulent and the Lushchik–Pavel'ev–Yakubenko three-equation turbulence model is used. It is so generalized that it allows for flow unsteadiness, complicated rheological properties, the presence of a free boundary, and the mass transfer at the lower flow boundary. The effect of the bottom material capture and the nonlinear rheological properties of the medium in motion on the flow dynamics is numerically investigated.

Keywords: downslope flows, turbulence, non-Newtonian fluids, slope material entrainment, mathematical modeling.

DOI: 10.1134/S0015462816030017

The naturally occurring flows on slopes, such as snow avalanches, mudflows, landslides, as well as lava and water flows, can constitute a danger for the public and structures. A knowledge of the dynamic parameters of these flows and the boundaries of their propagation zones is necessary for organizing the protection of different objects in mountains. One of the tools for obtaining this knowledge is mathematical simulation. The downslope flows can be described using the models of different levels [1]. In the simplest models the entire flow is considered as a material point moving along a slope under gravity and the resistance of the surrounding medium. In more sophisticated models the flow is regarded as the motion of a certain continuum. Thus, the models of hydraulic type were proposed and have been used; these are based on the depth- or cross-section-average equations with account for the approximations related with the fact that usually the characteristic flow depth (thickness) is much smaller than its streamwise scale. In this case, some formulas are postulated that relate the bottom friction and the bottom material capture rate with the depth and the mean longitudinal flow velocity. A review of these formulas is presented, for example, in [2]. These formulas cannot be derived from the consideration of physical processes in the bottom zone and the coefficients entering in them are empirical. Implicitly, they allow for not only the physical properties of media in motion but also the influence of different regional conditions. For this reason, the application of these models in practice is possible only after their preliminary calibration for typical slopes of a given region using the inverse calculations of actual flows.

The models of the third, more complicated level suggest the description of the flow parameter distributions throughout the entire flow on the basis of the complete equations of continuum mechanics. At present, such models have begun to be developed. In this case, the following problems arise. Firstly, this is the problem of constructing rheological relations for materials in motion. A very simple assumption consists

in that the material in motion can be described as a linearly-viscous, highly-viscous fluid. However, the measurements of the velocity profiles and the observable properties of downslope flows, for example, the capability of lava flows and landslides to stop on inclined slopes, indicate the necessity of using more complicated models. The second problem is associated with the fact that the downslope flows usually capture the material lying on the slope with the result that their mass can increase severalfold compared with the initial mass [3, 4]. The bottom material capture has a considerable effect on the ejected flow dimensions, dynamics, and range. In some cases, the thickness of the material layer stripped off by the downslope flow is of its own interest, for example, when the protection of cables and tubes placed under ground beneath the downslope flow path is designed. The mathematical model must include the law governing the bottom material entrainment. The third important problem is due to the fact that in many cases downslope flows are turbulent. The turbulence model must be selected, or developed, with account for the presence of a free surface and complicated nonlinear rheological properties of the medium in motion.

In this study, we consider the downslope flow models based on the complete (non-depth-average) equations. For the first time, the non-Newtonian medium properties, the capture of the bottom material, and the turbulence are taken into account together. The rheological properties of the material in motion are described by the so-called Herschel–Bulkley model [5], which can describe both linear and nonlinear viscous (power-law) fluids, as well as media with a yield strength, in particular, the Shvedov–Bingham fluid, by the appropriate choice of the coefficients. The Bingham and Herschel–Bulkley models were proposed as possible rheological models for snow avalanches, mudflows, lava flows, and landslides, for example in [6–12].

In this study, in modeling the bottom material capture we will use the following hypothesis, which will be called hypothesis A: the capture occurs, when the shear stress on the flow bottom reaches the value of the bottom material shear strength [12–15]. In this case, the bottom material entrainment rate is determined as a result of the calculations of the shear stress on the bottom in solving the problem. This hypothesis corresponds to a possible capture mechanism. It was put forward by many geoscientists who studied the motion of mudflows and landslides [4] and was formulated as a component part of the mathematical model of snow avalanches in [14, 15].

There has been much research, mostly experimental, of non-Newtonian turbulent fluid flows; see, for example, [16, 17] and the references therein. This is due to the fact that both in nature and in engineering flows moving in pipes and chutes and carrying suspended solid particles are widely encountered. They are used, in particular, in mining, chemical, food, and paper industries, in drilling oil wells, in producing polymers, and in sewage treatment plants. These flows exhibit non-Newtonian properties. For the engineering practice of main interest is the calculation of the pipeline and chute resistance. The above-mentioned studies deal with precisely this problem. Usually, they consider only steady flows and, on the basis of the experimental data, propose formulas for the resistance coefficient and the velocity profile, as well as the criteria of flow transition into the turbulent regime. In this case, the detailed flow structure is not considered. There are also a few studies using complete mathematical models of non-Newtonian turbulent flows on the basis of direct numerical simulation [18] or the preliminary Reynolds-averaging with employment of semi-empirical models [19]. In those studies steady flows in pipes and channels of fixed dimensions were considered without allowing for the possibility of the bottom material entrainment. In this study, the turbulent flow characteristics are described using the three-equation turbulence model proposed and applied for calculating fluid flows along impermeable and permeable walls in the presence of a pressure gradient, mass transfer, and other processes in [20–24]. The model was generalized to include the presence of a free surface in downslope flows, the unsteadiness due to, in particular, the bottom material capture, and the non-Newtonian properties of the medium in motion. The computational code was developed and the sets of calculations were carried out which showed the effect of the rheological properties and the material capture on the flow behavior.

1. FORMULATION OF THE PROBLEM

The main purpose of this study is to investigate the effect of the bottom material capture and the flow rheology and turbulence on its dynamics. In this connection, as in the previous papers [12–14] concerned

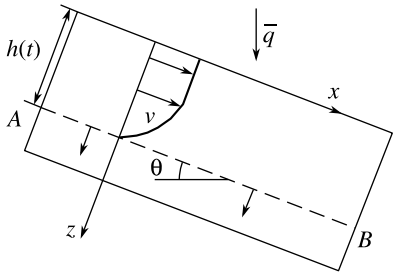

Fig. 1. Schematics of the flow; *AB* is the lower flow boundary and the bottom material breakdown front.

mainly with laminar flows, we accepted a very simple formulation of the problem in which a homogeneous flow on an infinitely long uniform slope with a constant angle θ is considered. The medium in motion is assumed to be incompressible, with a density $\rho = \rho_0 = \text{const}$. The origin is taken on the free surface of the flow, the x axis being aligned with the slope and the z axis being normal to it and downward directed (Fig. 1).

The Reynolds-averaged streamwise velocity and the other parameters depend only on z and time t, while the flow depth h varies with time if the flow captures the bottom material. The function $h(t)$ is to be determined.

For the flow under consideration the Reynolds equation can be written in the form:

$$\frac{\partial \langle v_x \rangle}{\partial t} = g \sin\theta + \frac{1}{\rho}\frac{\partial T_{xz}}{\partial z}, \qquad 0 \le z \le h(t). \tag{1.1}$$

Here, $T_{xz} = \langle \tau_{xz} \rangle + \rho T$ is the shear stress, or the sum of the average molecular stress $\langle \tau_{xz} \rangle$ and the turbulent stress ρT, where $T = -\langle v_x' v_z' \rangle$. The primes denote the fluctuational velocity components, while the angular brackets mean the Reynolds averaging. In what follows, we will omit the angular brackets in denoting the average values.

For all flows under consideration we will neglect the friction at the free surface $z = 0$

$$T_{xz} = 0, \qquad z = 0.$$

The no-slip conditions are imposed on the bottom $z = h(t)$

$$v_x = 0, \qquad z = h(t). \tag{1.2}$$

We note that in certain studies modeling geophysical downslope flows the no-slip condition at the bottom is replaced by different slip conditions [9–12, 25–27]. In particular, the measurements of the velocity profiles in dense snow flows [9, 26] show that the flow velocity is not small at very small distances from the bottom. However, so far there has not been reliable data on the slip law (if the slip must be taken into account) and, for this reason, in this study we use the no-slip condition.

Along with condition (1.2), for the flow capturing the bottom material, in accordance with the adopted hypothesis A on the capture, we impose an additional boundary condition on the bottom

$$|\tau_{xz}| = \tau_c, \qquad z = h(t), \tag{1.3}$$

where τ_c is the shear strength of the bottom material. This additional condition makes it possible to calculate the growing-in-time flow depth. We note that the lower surface of the flow can be treated as the phase transition front, where the bottom material breaks down and goes over into the flow material. However, as distinct from, for example, the Stefan problem, the boundary condition $\tau_{xz} = \tau_c$ does not explicitly include the front velocity. This requires the application of special approaches in calculating dh/dt.

Equation (1.1) must be supplemented with an expression for the molecular stress τ_{xz} and equations for T and other turbulence characteristics entering into the formulation of the turbulence model. We will first discuss the expressions for the molecular shear stress and its average value. The rheological relations can be different for problems different in their physical nature, such as dry and wet snow avalanches, snow-dust

avalanches, mudflows, landslides, volcanic lava flows, water flows, etc. The simplest assumption is that the flow can be described as the motion of an incompressible, linearly viscous fluid; in this case, $\tau_{ij} = 2\mu e_{ij}$, where $\mu = \text{const}$ and e_{ij} are the strain rate tensor components. For high-density snow avalanches this model was used in [10, 14, 25, 28–30]. However, the measurements of the velocity profiles in, for example, dense snow avalanches [9, 26, 31] and in mudflows, which are clay suspension flows with a high clay concentration [6], show the necessity of sophisticated nonlinear models. One of the possible models is that of Herschel and Bulkley [5] which is assumed to be applicable in describing many flows, both geophysical and those with suspended solid particles widely used in the mining and other industries [5–12, 16, 17, 32–34]. In accordance with this model, in a simple laminar shear flow the following relations are fulfilled: if $|\tau_{xz}| < \tau_0$, then $\partial v_x/\partial z = 0$. At $|\tau_{xz}| \geq \tau_0$ we have

$$|\tau_{xz}| = \tau_0 + K\left|\partial v_x/\partial z\right|^n.$$

These relations can be written in another form by introducing the viscosity coefficient μ as the ratio of the shear stress to the shear rate: $\tau_{xz} = \mu\partial v_x/\partial z$. Then if $|\tau_{xz}| < \tau_0$, then $\partial v_x/\partial z = 0$, while for $|\tau_{xz}| \geq \tau_0$ we have

$$\mu = \tau_0\left|\partial v_x/\partial z\right|^{-1} + K\left|\partial v_x/\partial z\right|^{n-1}. \tag{1.4}$$

Here, τ_0 is the yield strength (the medium does not deform until the shear stress is greater than τ_0) and K and n are some constants. For $\tau_0 = 0$ and $n = 1$ Eqs. (1.4) correspond to the linearly viscous fluid. At $\tau_0 \neq 0$ and $n = 1$ the medium is called the Bingham fluid and at $\tau_0 = 0$ and $n \neq 1$ it is the power-law fluid. If $n < 1$, which takes place, for example, for clay suspensions, the medium is called pseudoplastic. For an arbitrary motion, under the assumption that the medium is incompressible, Eqs. (1.4) are usually generalized as follows: $\tau_{ij} = 2\mu e_{ij}$. If $\sqrt{I_2(\tau)/2} < \tau_0$ then $\mu = \infty$, whereas, if $\sqrt{I_2(\tau)/2} \geq \tau_0$, we have

$$\mu = \frac{\tau_0}{\sqrt{2I_2(e)}} + K\left(\sqrt{2I_2(e)}\right)^{n-1}. \tag{1.5}$$

Here, $I_2(e) = \sum_{i,j} e_{ij}e_{ij}$ and $I_2(\tau) = \sum_{i,j} \tau_{ij}\tau_{ij}$ are the second invariants of the strain rate and "viscous" stress tensors.

The unsteady laminar downslope flows of media obeying the Herschel–Bulkley model with account for the slope material capture were considered in [12, 13]. In this study, we present the results of an investigation of turbulent flows. It is assumed that the average value of the molecular stress $\langle\tau_{xz}\rangle$ is related with the average velocity by Eqs. (1.4) and (1.5). This means, in particular, that the contribution made by the term $2\langle\mu' e'_{ij}\rangle$ is neglected. The assumptions of this type are used in all studies known to the authors and concerned with the modeling of turbulent flows of non-Newtonian fluids and describing the cross-sectional flow parameter distributions, for example, in [19, 32–34]. The construction of more complicated models including the necessary relations for $\langle\mu' e'_{ij}\rangle$ requires more complete experimental data on the flow structure.

To calculate the turbulent stresses and other turbulence parameters in this study we use the generalized three-equation Luschik–Pavel'ev–Yakubenko model [20] which in what follows will be denoted as the LPY model. The LPY model was developed and applied [20–24] for calculating flows of linearly viscous liquids and gases with constant or temperature-dependent viscosity along permeable and impermeable walls in the presence of heat transfer, convection, and other physical factors. The model includes the differential equations for three parameters, namely, the turbulent stress T divided by the density, the turbulent energy density $E = 0.5\langle v'_x v'_x + v'_y v'_y + v'_z v'_z\rangle$, and the parameter ω related with the turbulence scale L by the formula $\omega = E/L^2$. As distinct from the Prandtl model or, for example, the k–ε model, in the LPY model the Boussinesq hypothesis is not assumed and the relations for the turbulent viscosity are replaced by the equations for directly the turbulent stress T. This approach makes it possible to describe [35], in particular, the data of the experimental measurements [36] which show that there exist flows, for example, a flow in an

annular channel, where the turbulent shear stress is not zero at the points, where the shear rate vanishes. For the shear flow considered in this study the equations for T, E, and ω take the form:

$$\begin{aligned}
&\frac{\partial E}{\partial t} = -\big(c\sqrt{E}L + c_1\nu\big)\frac{E}{L^2} + \frac{\partial}{\partial z}\left(D_E\frac{\partial E}{\partial z}\right) + T\frac{\partial v}{\partial z},\\
&\frac{\partial T}{\partial t} = -(c_5\sqrt{E}L + c_6\nu)\frac{T}{L^2} + \frac{\partial}{\partial z}\left(D_\tau\frac{\partial T}{\partial z}\right) + c_7E\frac{\partial v}{\partial z},\\
&\frac{\partial \omega}{\partial t} = -\big(2c\sqrt{E}L + 1.4c_1\nu f_\omega\big)\frac{\omega}{L^2} + \frac{\partial}{\partial z}\left(D_\omega\frac{\partial \omega}{\partial z}\right) + \left[\frac{T}{E} + 2c_4\,\mathrm{sgn}\left(\frac{\partial v}{\partial z}\right)\right]\omega\frac{\partial v}{\partial z},\\
&D_\phi = a_\phi\sqrt{E}L + \alpha_\phi\nu \quad (\phi = E,\ T,\ \omega), \qquad f_\omega = 1 - \frac{1}{2c_1}\left(\frac{L}{E}\frac{\partial E}{\partial z}\right)^2.
\end{aligned} \tag{1.6}$$

Here, $v = v_x$ and $\nu = \mu/\rho$ is the kinematic coefficient of molecular viscosity. The values of the dimensionless coefficients are as follows: $c = 0.3$, $c_1 = 5\pi/4$, $c_4 = -0.04$, $c_5 = 3c$, $c_6 = 9c_1$, $c_7 = 0.2$, $a_E = a_\omega = 0.06$, $a_\tau = a_E c_5/c$, $\alpha_E = \alpha_\tau = 1$, and $\alpha_\omega = 1.4$. These values of the coefficients were used without any variations in calculating different flows, including the cases in which the viscosity coefficient μ was not constant but was a function of the variable temperature.

As the boundary conditions for T, E, and ω the following conditions at the bottom and the free surface were taken:

$$\begin{aligned}
z = h(t):&\quad T = 0, \qquad E = 0, \qquad \partial E/\partial z = 0,\\
z = 0:&\quad T = 0, \qquad \partial E/\partial z = 0, \qquad \partial\omega/\partial z = 0.
\end{aligned}$$

Thus, at the bottom the condition for ω was replaced by the additional condition for E. Many measurements in steady flows show that near a solid wall E is proportional to the square of the distance from the wall, that is, the condition $\partial E/\partial z = 0$ is fulfilled at the wall.

The complete formulation of the problem also includes the preassignment of the initial conditions. They have a considerable effect only on the initial stage of the motion; with time the flow along a homogeneous slope tends to become steady if there is no bottom material capture, while in the motion with the capture the flow depth and velocity increase and the initial data effect becomes inessential.

2. NEW FORMULATION OF THE PROBLEM

In numerically solving the problem the system of equations and boundary and initial conditions presented in the previous section was reformulated. Firstly, a new coordinate transverse to the slope, $z_1 = z/h(t)$ was introduced in order for the domain, in which the solution is sought, be known: $0 \le z_1 \le 1$. In the original formulation it is unknown: if the flow in motion strips off the bottom material, the flow depth $h(t)$ varies in an unknown fashion. The boundary condition (1.3) which must serve to determine $h(t)$ does not explicitly contain $h(t)$. In the new variables, the domain in which the solution is sought becomes fixed. In this case, in all the equations, including Eq. (1.3), there appear additional terms containing $h(t)$ and its time derivatives. Then condition (1.3) becomes the equation for determining $h(t)$. The second variation of the problem formulation consists in the regularization of the constitutive relations of the Herschel–Bulkley model. Namely, the expression for molecular viscosity in Eq. (1.4) at $\tau_0 \ne 0$ was replaced by the condition: if $|\partial v_x/\partial z| < \varepsilon$, then $\mu = \tau_0/\varepsilon$; otherwise

$$\mu = (\tau_0 - K\varepsilon^n)\big|\partial v_x/\partial z\big|^{-1} + K\big|\partial v_x/\partial z\big|^{n-1}.$$

Here, ε is a small quantity. Finally, all the equations were rewritten in dimensionless variables,which are below referred to by the subscript "1"

$$\begin{aligned}
&z_1 = \frac{z}{h(t)}, \quad t_1 = \frac{t}{t_*}, \quad v_{x1} = \frac{v_x}{v_*}, \quad h_1 = \frac{h}{h_*}, \quad \tau_{01} = \frac{\tau_0}{\tau_c}, \quad \tau_{xz1} = \frac{\tau_{xz}}{\tau_c},\\
&\mu_1 = \frac{\mu}{\mu_*}, \quad \varepsilon_1 = \frac{\varepsilon}{\varepsilon_*}, \quad E_1 = \frac{E}{v_*^2}, \quad T_1 = \frac{T}{v_*^2}, \quad \omega_1 = \omega\frac{h_*^2}{v_*^2}, \quad L_1 = \frac{L}{h_*}.
\end{aligned} \tag{2.1}$$

Here and in what follows

$$v_* = \sqrt{\frac{\tau_c}{\rho}},\ \ h_* = \frac{v_*^2}{g},\ \ t_* = \frac{v_*}{h_*},\ \ \varepsilon_* = \frac{v_*}{h_*},\ \ \mu_* = K\left(\frac{v_*}{h_*}\right)^{n-1},\ \ \nu_* = \frac{\mu_*}{\rho},\ \ \mathrm{Re}_* = \frac{v_* h_*}{\nu_*}. \tag{2.2}$$

We note that $h_* = h_{sl}\sin\theta$, where h_{sl} is the depth of a steady flow in which the stress at the bottom is τ_c. A steady flow with a depth $h > h_{sl}$ and the bottom stress τ_c is impossible. If the initial flow depth $h_0 > h_{sl}$, then the flow will be unsteady, with the bottom material destruction and its entrainment into the motion, at the expense of which the flow depth and, therefore, the linear scale, will increase. The "Reynolds number" Re_* introduced in Eq. (2.2) is constant and does not characterize the unsteady flow properties. We note that, owing to the fact that non-Newtonian fluid flows in pipes and chutes are widely used in practice, the question of how the dimensionless quantities determining the boundaries of the laminar and turbulent regimes and the resistance coefficient of a pipe or a channel should be introduced is being discussed up to present. One of the possible expressions for the Reynolds number proposed for steady turbulent flows of the fluids with the rheological equation (1.5) in wide channels is written in the form:

$$\mathrm{Re}_2 = \frac{8\rho v_{av}^2}{\tau_0 + K(2v_{av}/h)^n},$$

where v_{av} is the depth-average velocity. Then in the steady laminar flow regime the following relation for the resistance coefficient λ is fulfilled: $\lambda = 64/\mathrm{Re}_2$ [16, 17]. In our calculations Re_2 was calculated, together with the Reynolds number $\mathrm{Re}_{\mathrm{mean}}$ based, in accordance with the usual expression, on the depth and the depth-average values of the velocity and kinematic viscosity: $\mathrm{Re}_{\mathrm{mean}} = v_{av}h/\nu_{av}$. In describing fluids with a yield strength one more dimensionless parameter is introduced, namely, $B = \tau_0 h_*^n/(K v_*^n)$.

Below the Reynolds equation, the formulas for molecular viscosity, and the boundary conditions for the velocity are written down in the dimensional form. In these relations it is taken into account that $z_1 = z/h(t) = z_1(h,\ t)$. the designation $v_x = v$ is introduced, and the subscript "1" is omitted here and in what follows

$$\frac{\partial v}{\partial t} = \frac{\partial v}{\partial z}\frac{z}{h}\frac{dh}{dt} + \sin\theta + \frac{1}{\rho h^2 \mathrm{Re}_*}\frac{\partial}{\partial z}\left(\mu\frac{\partial v}{\partial z} + \rho T\right), \quad 0 \le z \le 1,$$

$$\begin{cases} \text{If } |\partial v/\partial z| < \varepsilon h, \quad \text{then} \quad \mu = \tau_0 \mathrm{Re}_*/\varepsilon; \\ \text{If } |\partial v/\partial z| \ge \varepsilon h, \quad \text{then} \quad \mu = h\big(\tau_0 \mathrm{Re}_* - \varepsilon^n\big)\left|\dfrac{\partial v}{\partial z}\right|^{-1} + \left|\dfrac{\partial v}{\partial z}\right|^{n-1}\dfrac{1}{h^{n-1}}, \end{cases} \tag{2.3}$$

$$z = 0:\ \frac{\partial v}{\partial z} = 0, \qquad z = 1:\ v = 0, \quad \frac{\mu}{\mathrm{Re}_*}\frac{\partial v}{\partial z} = h.$$

The last relation (2.3) is a new form of condition (1.3). It represents the relationship between the flow depth and the derivative of the velocity normal to the bottom. The other equations and conditions of the problem are transformed in the similar fashion. For example, Eq. (1.6) takes the form:

$$\frac{\partial E}{\partial t} = \frac{\partial E}{\partial z}\frac{z}{h}\frac{dh}{dt} - \left(c\sqrt{E}L + \frac{c_1\nu}{\mathrm{Re}_*}\right)\frac{E}{L^2} + \frac{1}{h^2}\frac{\partial}{\partial z}\left(D_E\frac{\partial E}{\partial z}\right) + \frac{1}{h}T\frac{\partial v}{\partial z}, \quad D_E = a_E\sqrt{E}L + \frac{\alpha_E\nu}{\mathrm{Re}_*}.$$

3. RESULTS OF THE NUMERICAL INVESTIGATION

For numerically modeling the flow behavior on the basis of the mathematical model formulated the calculation method using an implicit difference scheme was developed. At each time step the calculations were performed using the matrix sweep technique with an iteration procedure.This is due to the problem nonlinearity and the specific features of the boundary conditions, in particular, the necessity to calculate the new flow depth, such that the bottom friction would be τ_c, and the fact that the quantity ω is not preassigned at the bottom, while two boundary conditions are specified for E. The computational code was developed and

the sets of calculations of turbulent, steady and unsteady, flows of media with different rheological properties, moving with and without the bottom material capture were carried out. The profiles of the velocity, the turbulent energy, and other parameters were obtained, as well as time dependences of the maximum and cross-section-average velocities, the Reynolds numbers, the flow depth, and the bottom material entrainment rate. The examples of the calculated results are presented in Figs. 2–6. Some dependences are plotted in the dimensionless variables determined by Eqs. (2.1) and (2.2). On the other plots the results are presented in the dimensional variables. This is done in order for the calculated values of the flow velocities and the bottom material entrainment rates could be compared with the available data of measurements of actual flows. In some figures the parameter distributions in a flow cross-section are plotted against a dimensionless coordinate y^+, which is determined by generalizing the formula conventionally used in describing steady turbulent flows of Newtonian fluids in terms of the dimensional and dimensionless variable, respectively

$$y^+ = \frac{v_\tau}{\nu_b}(h - z) = \mathrm{Re}_* \frac{v_{\tau 1}}{\nu_{b1}} h_1 (1 - z). \tag{3.1}$$

Here, $v_\tau = \sqrt{|\tau_b|/\rho}$, τ_b, and ν_b are the molecular stress and kinematic viscosity at the bottom and the quantities with the subscript "1" are introduced in accordance with Eqs. (2.1) and (2.2). For the fluids described by the Herschel–Bulkley models expression (3.1) for y^+ can be rewritten in terms of the formula for ν_b in the form:

$$y^+ = \frac{\left(|\tau_b| - \tau_0\right)^{1/n}}{K^{1/n}\sqrt{|\tau_b|/\rho}}(h - z) = \mathrm{Re}_*^{1/n} \frac{\left(|\tau_{b1}|/\rho_1 - \tau_{01}/\rho_1\right)^{1/n}}{\sqrt{|\tau_{b1}|/\rho_1}} h_1 (1 - z_1).$$

When using the coordinate y^+ the dimensionless velocity, turbulent stress, and turbulent fluctuation energy are introduced basing on the quantity v_τ

$$v^+ = v/v_\tau, \qquad T^+ = T/v_\tau^2, \qquad E^+ = E/v_\tau^2. \tag{3.2}$$

We note that in unsteady flows the quantities τ_b and, in the case of non-Newtonian fluids, also ν_b are time-dependent and are not known beforehand. In the motion with the bottom material capture, in accordance with the adopted hypothesis A, $\tau_b = \tau_c$, where τ_c is a given quantity.

Figures 2, 3, and 4I pertain to the calculations of turbulent flows of linearly viscous fluids. The effect of the initial data, the slope inclination, viscosity, and the bottom material strength on the dynamic parameters and the bottom material capture rate was studied. The results presented in Figs. 2, 3, and 4I were obtained for the following values of the input parameters selected on the basis of the data on snow avalanches and the snow coating strength [3, 8, 9, 14, 25, 28, 29]

$$\tau_0 = 0,\ n = 1,\ K/\rho \equiv \nu = 10^{-3}\ \mathrm{m^2 s^{-1}},\ \theta = 30^\circ,\ \tau_c/\rho = 1.5\ \mathrm{m^2 s^{-2}},\ h(0) = 1\ \mathrm{m},\ v(0,\ z) = 0. \tag{3.3}$$

In this case, $\mathrm{Re}_* = 187.3$, $h_* = 0.153$ m, and $v_* = 1.225$ m/s.

In Fig. 2 the results of the calculations of the unsteady flow without the bottom material capture are presented. The left boundary is the bottom and the right one is the free boundary; $1 - z$ is the ratio of the distance from the bottom to the total flow depth. The turbulent parameter profiles are presented for three moments of time in the dimensionless variables (2.1) and in the "wall" variables (3.1) and (3.2). The corresponding values of the Reynolds number at these moments $\mathrm{Re}_{\mathrm{mean}} = 41338$, 49327, and 50328.

Clearly that, when the flow moves without the bottom material capture along a long homogeneous slope, then a steady flow regime is attained with time. We note that in any steady uniform downslope flow of fixed depth h the bottom friction $\tau_b = \rho g h \sin\theta$. For the input parameters (3.3) this quantity is greater than τ_c which contradicts the adopted hypothesis A, in accordance with which $\tau_b \le \tau_c$. This means that, as the flow develops, it necessarily begins to capture the bottom material. To analyze the flow development in the absence of the bottom material capture, the capture was prohibited by the special command of the code.

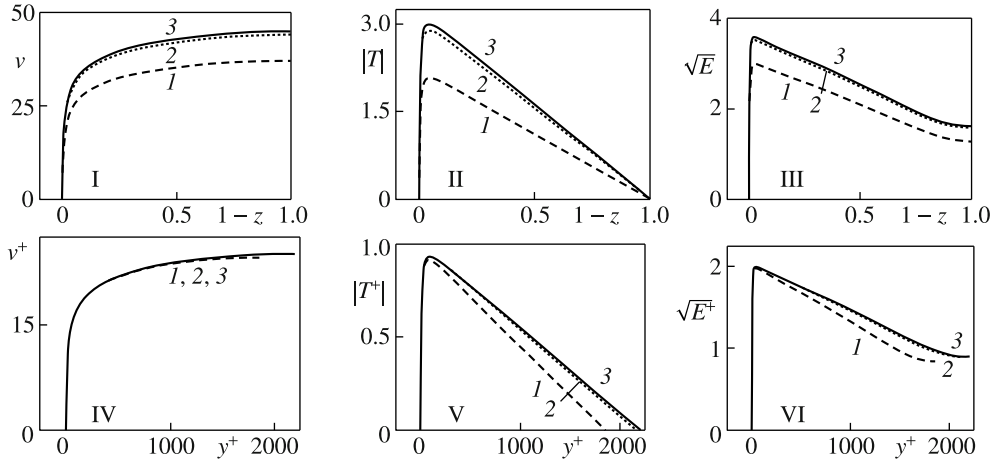

Fig. 2. Turbulent flow of the linearly viscous fluid without the bottom material capture. Profiles of the velocity, the turbulent stress, and square root of the turbulent energy at the moments $t = 100$, 200, and 300 s (*1–3*); I–III, in the dimensionless variables (2.1) and (2.2) and IV–VI, in the wall variables (3.1) and (3.2).

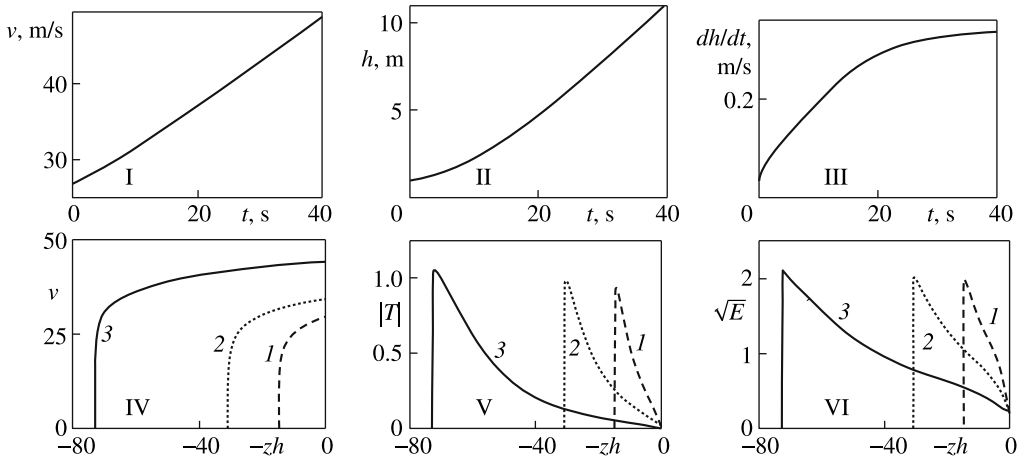

Fig. 3. Turbulent flow of the linearly viscous fluid with the bottom material capture. I–III, time dependences of the dimensional cross-section-average velocity, flow thickness, and bottom material capture rate, time is measured from the onset of the capture; IV–VI, dimensionless velocity, turbulent stress, and square root of the turbulent energy as functions of the dimensional distance from the free surface at the moments $t = 10$, 20, and 30 s (*1–3*).

The calculations show that in a thin near-bottom layer the velocity profile takes the form $v^+ = y^+$ not only in steady but also in unsteady flows, this being true for flows of different rheology, with and without the bottom material capture (Fig. 4). In the turbulent flow of a linearly viscous fluid without the bottom material capture the $v^+(y^+)$ dependences for the entire cross-section plotted in unsteady motion at different moments of time lie on almost the same curve (Fig. 2IV). In the main flow the turbulent stress T^+ and the turbulent energy density E^+ increase with increase in the flow velocity but their maximum values remain constant.

The examples of the calculated turbulent flows of a linearly viscous fluid capturing the bottom material with the input parameters (3.3) are presented in Figs. 3 and 4I. In this case, the motion is essentially unsteady. In Fig. 3 the time dependences of the dimensional cross-section-average velocity v_{av}, the flow depth h, and the bottom material capture rate dh/dt are presented (I–III). The turbulent parameter distributions in the flow cross-section (IV–VI) are plotted in Fig. 3 as functions of the coordinate zh which is the dimensionless, that is, divided by the quantity $h_* = 0.153$ m, distance from the free surface whose equation is $z = 0$. With the bottom material capture the distance from the bottom increases and the left flow boundary in Fig. 3IV–3VI, moves leftward with time.

Clearly that, at the expense of the material entrainment, the cross-section-average velocity and the flow thickness increase with time, the dependence $h(t)$ approaching to the linear dependence, so that the bottom

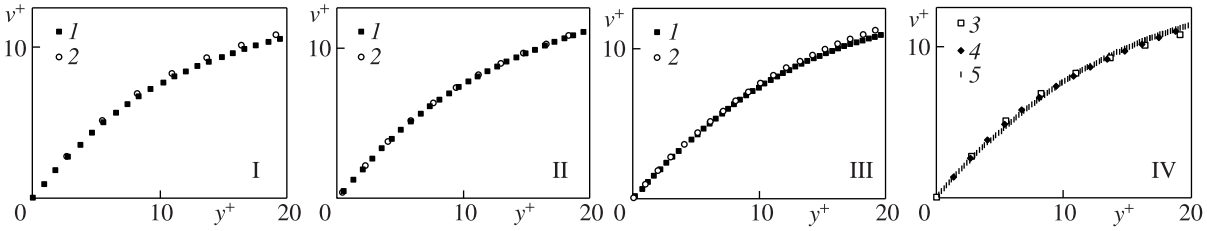

Fig. 4. Velocity profiles in the wall variables in the bottom region of turbulent flows moving with the bottom material capture at the moments $t = 20$ s (*1*) and 30 s (*2*); I linearly viscous fluid, II Bingham fluid, III power-law fluid, and IV comparison of the velocity profiles at the moment $t = 30$ s in the flows of media with different rheologies: (*1*) linearly viscous fluid, (*2*) Bingham fluid, and (*3*) power-law fluid.

material capture rate tends to a constant dependent only on the properties of the material in motion and the slope. The turbulent stress T and the turbulent fluctuation energy E in the particles at a given distance from the free surface decrease, while the maximum values of T and E occurring near the bottom increase, the maximum points themselves slightly moving from the bottom toward the main flow. We note that in all calculations performed neither restrictions on the amount of the captured material and, therefore, the flow thickness growth, were imposed. This made it possible to determine the asymptotic behavior of the capture rate in motion along the long homogeneous slope. In practice, the flow thickness h growth is restricted by virtue of two reasons. Firstly, the bottom material layer, which can be entrained in the motion, is usually of finite thickness and, secondly, the flow time is also bounded. For example, for a snow avalanche, provided it does not strip off the ground, the entrained layer thickness cannot be greater than the snow coating thickness, while the time of motion is measured by seconds.

In the bottom zones the velocity profiles $v^+(y^+)$ of turbulent linearly- viscous, Bingham, and power-law fluid flows moving with the bottom material capture are presented in Fig. 4I–4III for different moments of time. The calculations are carried out with the input parameters (3.3), (3.5), and (3.6), respectively. Time is measured from the onset of the bottom material capture. In Fig. 4IV these profiles are compared for all the three media in motion.

In laminar flows of Newtonian and non-Newtonian fluids, in which the molecular viscous stresses are functions of the strain rates, while the material capture occurs in accordance with hypothesis A, in the motion along a long homogeneous slope, a near-bottom zone with the linear velocity profile is formed. Its thickness increases proportional to time, so that at large times this zone occupies almost the entire flow cross-section, while the bottom material capture rate tends to a constant value [12–14]. In [12, 13] the asymptotic (as $t \to \infty$) formulas for the velocity profile in the expanding bottom zone and the bottom material capture rate dh/dt were proposed for laminar flows. For the media governed by the Herschel–Bulkley models they have the following dimensional form:

$$v_x = \left(\frac{\tau_c - \tau_0}{K}\right)^{1/n}(h - z), \qquad \frac{dh}{dt} = \frac{K^{1/n} g \sin\theta}{(\tau_c - \tau_0)^{1/n}}. \tag{3.4}$$

Formula (3.4) for the velocity profile can be written in the form $v^+ = y^+$. In turbulent flow with the bottom material capture there is also a narrow near-bottom zone with the linear velocity profile $v^+ = y^+$ but it does not expand with time. In the bottom region there arises a nonlinear velocity profile, which is universal in the "bottom" variables v^+, y^+, that is, it depends on neither time nor the rheology of the media considered (Fig. 4). Formula (3.4) for the asymptotic capture rate derived for laminar flows is inapplicable for turbulent flows. For example, for the flow of the linearly viscous fluid with the input parameters (3.3) it gives the asymptotic value $dh/dt = 0.0033$ ms^{-1} which is two orders smaller than that obtained in the calculations (Fig. 3III).

The results of an investigation of non-Newtonian fluid flows are presented in Figs. 4 (II and III) to 6. In Fig. 5 an example of the calculations of the power-law fluid flow is presented (Ostwald–de Ville model, or a particular case of the Herschel–Bulkley model). The calculations were performed for the following

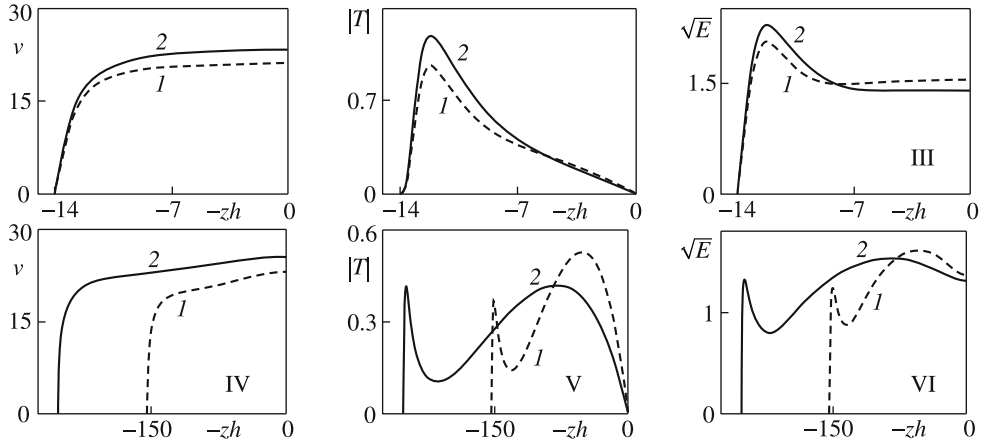

Fig. 5. Turbulent flows of the power-law fluid with the exponent $n = 2$. Dimensionless parameter distributions in the cross-section in flows moving without (I–III) and with (IV–VI) the bottom material capture at the moments (*1* and *2*) (onset of the capture at $t = 7$ s); zh is the distance from the free surface divided by $h_* = 0.07$ m.

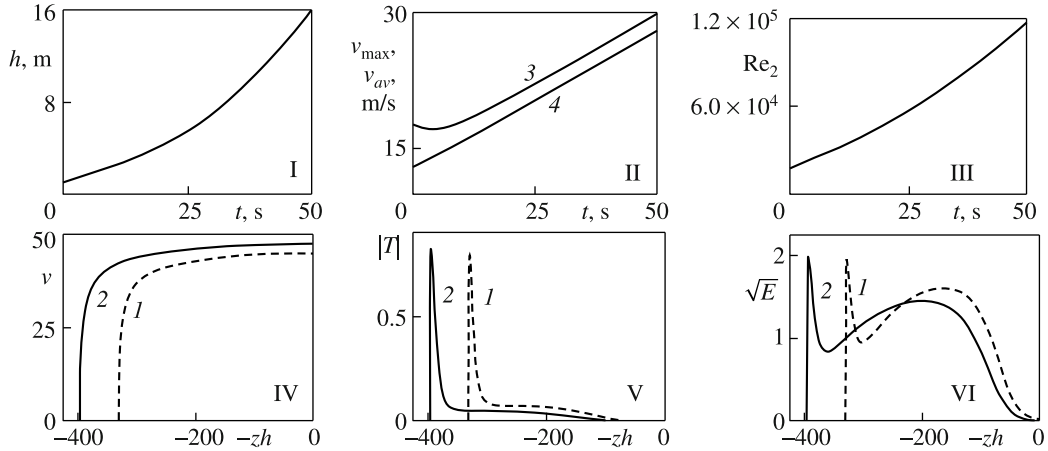

Fig. 6. Turbulent flow of the Bingham fluid with the bottom material capture; I–III, time dependences of the dimensional flow thickness, maximum (II, *3*) and cross-section-average (II, *4*) velocities, and the Reynolds number Re_2; time is measured from the onset of the capture; IV–VI, dimensionless velocity, turbulent stress, and square root of the turbulent energy density as functions of the dimensionless distance from the free surface at the moments $t = 45$ and 50 s (*1*, *2*).

values of the input parameters

$$n = 2, \quad \tau_0 = 0, \quad K/\rho = 0.0001\ \mathrm{m^2\,s^{-1}}, \quad \tau_c/\rho = 0.7\ \mathrm{m^2\,s^{-2}}, \quad \theta = 30^\circ, \quad h(0) = 1\ \mathrm{m}. \tag{3.5}$$

In this case, $h_* = 0.07$ m and $v_* = 0.84$ m/s. The exponent $n = 2$ was proposed in [9] on the basis of the experiments on modeling dense snow avalanches.

In the flow without the material capture the profiles of the velocity and the turbulence parameters in the power-law fluid flow are qualitatively similar with those in the linearly viscous fluid flow (Fig. 5I–5III). With time the velocities, the turbulent stresses, and the turbulent energy density increase approaching some steady distributions. In the flow with the material capture, if the initial data are such, that the flow initially accelerates without the bottom material capture until the bottom stress reaches the value τ_c and only then the capture begins, the arising turbulence parameter profiles have two local maxima, one of which is located near the bottom, while the other is the central part of the flow (Fig. 5IV–5VI). As the material capture is continued, the turbulent parameters at points of maximum increase near the bottom and decrease in the main flow.

An example of the calculations of unsteady flow of a fluid possessing the yield strength, namely, the viscoplastic Bingham fluid, with the bottom material entrainment is shown in Fig. 6. The calculations were carried out for the following set of the input parameters

$$n = 1,\ \tau_0/\rho = 0.05\ \mathrm{m^2 s^{-2}},\ \tau_c/\rho = 0.4\ \mathrm{m^2 s^{-2}},\ \theta = 30^\circ,\ \mu/\rho = 0.001\ \mathrm{m^2 s^{-1}},\ h(0) = 1\ \mathrm{m}. \tag{3.6}$$

In this case, $h_* = 0.04$ m and $v_* = 0.63$ m/s.

Figure 6I and 6II shows that in the Bingham fluid flow along a long homogeneous slope with the bottom material capture, in accordance with hypothesis A, as in the linearly viscous and power-law fluid flows, the velocity and the flow thickness increase with time and at large t their time dependences are near-linear. From the plots in Fig. 6V and 6VI, it can be seen that in the turbulent Bingham flows, as in the power-law fluid flows, when a flow for a certain time accelerated without the bottom material capture, with the onset of the capture there appear the turbulent parameter profiles with two local maxima. Due to the presence of the yield strength, a layer moving without deformations, as a solid crust, appears and develops near the free surface, where tangent stresses are small. Correspondingly, the calculations show that the turbulent stresses and energy are small not only near the solid bottom but also near the free surface (Fig. 6VI).

Summary. In this study unsteady turbulent downslope flows of Newtonian and non-Newtonian fluids capturing in motion the bottom material are for the first time modeled using the equations non averaged over the depth. In calculating the turbulence parameters the generalized differential three-equation Lushchik–Pavel'ev–Yakubenko model is used. It is assumed that the bottom material capture occurs, when the shear stress in the bottom flow reaches the shear strength of the bottom material (hypothesis A). The main conclusions obtained in analyzing the calculated results for flows along homogeneous slopes are as follows. At the expense of the bottom material capture, the flow velocity and thickness increase. In motion along a long homogeneous slope with the bottom material capture at large times the velocity at the flow surface, the cross-section-average velocity, and the flow depth increase linearly with time, irrespective of the rheological properties of the flow. The bottom material capture rate tends with time to a constant value which depends only on the slope inclination and the physical properties of the flow and slope materials but is independent of the current values of the mean velocity and the depth. In motion with the bottom material capture the turbulent stresses and energy decrease with time almost everywhere, whereas the maximum, near-bottom values increase. In the Bingham and power-law ($n > 1$) fluid flows capturing the bottom material the turbulence parameters may have two rather than one local maxima in the cross-section, one of which is located near the bottom and the other is the medium part of the flow cross-section. The molecular viscosity has an effect on the turbulent parameter distributions in the flow cross-section. In flows with different rheological properties the turbulent parameter profiles are qualitatively different. In the Bingham fluid flows the turbulent stresses and energy, as well as the turbulence scale, can be small not only near the solid bottom but also near the free surface, where the shear stresses are small and the medium moves as a solid crust.

The authors wish to thank A.G. Kulikovskii for discussion of the questions considered in this study.

The study was carried out with the support of the Russian Foundation for Basic Research (projects Nos. 13-08-00084 and 15-01-00361).

REFERENCES

1. M.E. Eglit, "Theoretical Approaches to the Calculations of the Snow Avalanche Motion," in: *Advances in Science and Engineering. All-Union Institute of Science and Technical Information. Ground Hydrology and Glaciology Series.* [in Russian], Moscow (1968), p. 60.
2. M.E. Eglit and K.S. Demidov, "Mathematical Modeling of Snow Entrainment in Avalanche Motion," Cold Regions Sci. Technol. **43**, 10 (2005).
3. B. Sovilla, P. Burlando, and P. Bartelt, "Field Experiments and Numerical Modeling of Mass Entrainment in Snow Avalanches," J. Geophys. Res. **111**(F03007), 1 (2006).
4. O. Hungr, S. McDougall, and M. Bovis, *Entrainment of Material by Debris Flows*, Springer, Berlin (2005).
5. W.H. Herschel and R. Bulkley, " Über die Viskosität und Elastizität von Solen," Ann. Soc. Testing Mater. **26**, 621 (1923).
6. P. Coussot, *Mudflow Rheology and Dynamics*, Balklema Publ., Rotterdam (1997).
7. X. Huang and M.H. Garcia, "A Herschel–Bulkley Model for Mud Flow down a Slope," J. Fluid Mech. **374**, 305 (1998).
8. D. Issler, "Experimental Informations on Snow Avalanches," in: K. Hutter and N. Kirchner (eds.), *Dynamic Response of Granular and Porous Materials under Large and Catastrophic Deformations*, Springer, Berlin (2003), p. 109.

9. M. Kern, F. Tiefenbacher, and J. McElwaine, "The Rheology of Snow in Large Chute Flows," Cold Regions Sci. Technol. **39**, 181 (2004).
10. E. Bovet, C. Chiaia, and L. Preziosi, "A New Model for Snow Avalanche Dynamics Based on Non-Newtonian Fluids," Meccanica **45**, 753 (2010).
11. N.J. Balmforth, A.S. Burbidge, R.V. Craster, J. Salzig, and A. Shen, "Visco-plastic Models of Isothermal Lava Domes," J. Fluid Mech. **403**, 37 (2000).
12. M.E. Eglit and A.E. Yakubenko, "Numerical Modeling of Slope Flows Entraining Bottom Material," Cold Regions Sci. Technol. **108**, 139 (2014).
13. M.E. Eglit, A.E. Yakubenko, and T.A. Yakubenko, "Numerical Modeling of an Unsteady Flow of a Nonlinear Viscous Fluid," in: *Models and Methods of Aerodynamics. Materials of 13-th International Workshop* [in Russian], Moscow (2013), p. 218.
14. D. Issler and M. Pastor Pérez, "Interplay of Entrainment and Rheology in Snow Avalanches; a Numerical Study," Annals of Glaciology **52**, 143 (2011).
15. D. Issler, "Dynamically Consistent Entrainment Laws for Depth-Averaged Avalanche Models," J. Fluid Mech. **759**, 701 (2014).
16. P.T. Slatter, "Modeling the Turbulent Flow of Non-Newtonian Slurries," R & D Journal, **12** (2), 68 (1996).
17. R.P. Chhabra and J.F. Richardson, *Non-Newtonian Flow and Applied Rheology*, Elsevier, Oxford (2008).
18. M. Rudman and H.M. Blackburn, "Direct Numerical Simulation of Turbulent Non-Newtonian Flow Using a Spectral Element Method," Apl. Math. Modeling **30**, 1229 (2006).
19. M. Nakamura and T. Sawada, "A k–ε Model for Turbulent Analysis of Bingham Plastic Fluid in a Pipe," Trans. Jap. Soc. Mech. Eng. **B52** (479), 2544 (1986).
20. V.G. Lushchik, A.A. Pavel'ev, and A.E. Yakubenko, "Three-Parameter Model of Shear Turbulence," Fluid Dynamics **13** (3), 350 (1978).
21. V.G. Lushchik, A.A. Pavel'ev, and A.E. Yakubenko, "Three-Parameter Model of Turbulence: Heat Transfer Calculations," Fluid Dynamics **21** (2), 200 (1986).
22. V.G. Lushchik and A.E. Yakubenko, "Comparative Analysis of Turbulence Models for Calculating a Near-Wall Boundary Layer," Fluid Dynamics **33** (1), 36 (1998).
23. V.G. Lushchik and A.E. Yakubenko, "Friction and Heat Transfer in the Boundary Layer on a Permeable Surface in the Case of Foreign Gas Injection," Teplofiz. Vys. Temp. **43**, 880 (2005).
24. A.I. Leontiev, V.G. Lushchik, and A.E. Yakubenko, "A Heat-Insulated Permeable Wall with Suction in a Compressible Gas Flow," Int. J. Heat Mass Transfer **52** (17–18), 4001 (2009).
25. T.E. Lang and J.D. Dent, "Scale Modeling of Snow Avalanche Impact on Structures," J. Glaciology **26** (94), 189 (1980).
26. M. Naaim, F. Naaim-Bouvet, T. Faug, and A. Bouchet, "Dense Snow Avalanche Modeling: Flow, Erosion, Deposition and Obstacle Effects," Cold Regions Sci. Technol. **39**, 193 (2004).
27. E.A. Vedeneeva, "Lava Spreading during Volcanic Eruptions on the Condition of Partial Slip along the Underlying Surface," Fluid Dynamics **50** (2), 203 (2015).
28. J.D. Dent and T.E. Lang, "Modeling of Snow Flow," J. Glaciology **26** (94), 131 (1980).
29. J.D. Dent and T.E. Lang, "Experiments on the Mechanics of Flowing Snows," Cold Regions Sci. Technol. **5** (3), 253 (1982).
30. K. Nishimura and N. Maeno, "Contribution of Viscous Forces to Avalanche Dynamics," Annals of Glaciology, **13**, 202 (1989).
31. J.D. Dent, K.J. Burrel, D.S. Schmidt, M.Y. Louge, E.E. Adams, and T.G. Jazbutis, "Density, Velocity and Friction Measurements in Dry-Snow Avalanche," Annals of Glaciology, **26**, 247 (1998).
32. T. Juha-Pekka, R. Huhtanen, and J. Karvinen, "Interaction of Non-Newtonian Fluid Dynamics and Turbulence on the Behavior of Pulp Suspension Flows," Annual Transactions of the Nordic Rheology Society, **13**, 177 (2005).
33. A.A. Gavrilov and V.Ya. Rudyak, "A Model of Averaged Molecular Viscosity for Turbulent Flow of Non-Newtonian Fluids," J. Siberian Federal Univ. Math. & Phys. **7** (1), 46 (2014).
34. J. Khorshidi, S. Niazi, H. Davari, M. Abyaneh, and A. Mahmoodzadeh, "Turbulent Modeling for Non-Newtonian Fluid in an Eccentric Annulus," Canadian J. Pure Appl. Science, **7**, 2425 (2013).
35. A.E. Yakubenko, "Development of the Three-Equation Differential Turbulence Model and Investigation of Flows of Liquids, Gases, and Electroconducting Media on its Basis" [in Russian], Moscow State Univ., Dissertation (1991).
36. K. Hanjalic and B.E. Launder, "Contribution towards a Reynolds-Stress Closure for Low-Reynolds-Number Turbulence," J. Fluid Mech. **74**, 593 (1976).